DOI: 10.48011/sbse.v1i1.2182

Reactive power control of DFIG-based wind turbines for voltage support during faults

João Paulo Man Kit Sio * **Romeu Reginatto** **

* *Center for Engineering and Exact Sciences, Western Paraná State University - UNIOESTE, PR, (e-mail: joao.sio@unioeste.br).*
** *Center for Engineering and Exact Sciences, Western Paraná State University - UNIOESTE, PR, (romeu@unioeste.br)*

Abstract: The wind power penetration in the power system has already reached a considerate proportion. An important step in that path was the requirement of wind farms to provide Low Voltage Ride Through (LVRT) capacity, remaining connected to the grid during faults. More recently, grid codes are also requiring wind turbines to inject reactive power during the fault event so as to contribute to grid voltage support. The purpose of this work is to analyze a reactive current injection strategy for DFIG-based wind turbines that acts on the reactive power control loop during faults. The results of the simulations show, the behavior of the voltage, active power, and the total current injected in the system for different connection characteristics. The reactive current injection strategy helps in the voltage level during the fault, and the effectiveness is better for connections to the transmission system level.

Keywords: DFIG, Fault, Reactive power control, Wind power, Wind turbine.

1. INTRODUCTION

In the last decades, Wind Energy Conversion Systems (WECS) have become popular due to the environmental care, in particular, the Doubly Fed Induction Generator (DFIG) wind turbine (WT) due to the low cost compared to the full-scale converter wind turbine. The increase in wind power penetration in the power system made topics to emerge, such as reliability, stability, and quality enhancement.

In order to rely on the wind farm during system faults, many techniques have been studied to support and keep the wind turbine connected to the grid. These techniques give the WT the Low Voltage Ride Through (LVRT) capacity, and it has shown good results in keeping the generator connected and not tripping. However, only LVRT does not support the grid voltage during a fault.

Grid codes of several countries such as Denmark, Germany, Ireland, among others, already require reactive current injection for grid voltage support during a short circuit event (Asif et al., 2018). See, for instance, (Nycander and Söder, 2018) for comparison of the requirements of different countries, which differ in term of active power recovery, LVRT capacity, droop range, and other variables.

An approach to have a grid voltage enhancement is proposed by Kim et al. (2016), where an adaptive hierarchical voltage control of a Doubly Fed Induction Generator (DFIG) to secure a higher amount of reactive power in the wind farm during the grid fault event. The Q-V characteristic method proposed by Kim et al. (2016) changes temporally depending on the reactive power available at the DFIG.

Asif et al. (2018) proposes an enhanced LVRT capacity strategy, where an improved decoupled RSC-GSC strategy is adopted and the Chinese grid code requirement is considered. The method chosen, is to decouple the converter and improve the LVRT capacity and supporting the grid voltage due to reactive power injection. The method is to change the reactive power reference and the grid side converter quadrature current reference depending on the grid voltage value.

Reactive current injection during faults has been recently incorporated as a requirement by the Brazilian National System Operator (ONS) (ONS, 2019). Based on the Brazilian grid code this work will focus on evaluating the voltage support, by injecting reactive current, varying the reactive power reference in the Rotor Side Converter (RSC), following a strategy similar to Asif et al. (2018). Dynamic performance is analyzed by simulations, where the value of X/R and the integration level (ρ) will assume different values.

This type of simulation will provide the behavior of grid voltage, total current, active, and reactive power provided by the WT. The simulation took place in the distribution grid to evaluate the behavior of the reactive power control of a WT in that type of grid. The WT used in the simulation is a DFIG-based wind farm with $20MW$ of power capacity.

2. WIND TURBINE MODEL

The wind turbine model is presented in five separated parts. In this section, it will be shown briefly how each part is modeled: wind , turbine , the mechanical coupling , induction generator, converter model, and also the control system.

The wind is modeled as a constant value due to the interest of the analysis and the low impact of its variation on the dynamics during a fault. Furthermore, the turbine aerodynamic model can be described into three different approaches, the Blade Element Momentum Method (BEM), the algebraic approximation through performance coefficient, and wind turbine power curve approximation. In this paper, the turbine is modeled with the algebraic approximation method. This method is more simplified than the BEM method but more accurate than the power curve approximation method. To be able to obtain the C_p value it is used the following equations (**?**)

$$C_p(\lambda_t, \beta) = a_1 \left(\frac{a_2}{\lambda_i} - a_3\beta - a_4\beta^{a_5} - a_6 \right) e^{\frac{-a_7}{\lambda_i}} \quad (1)$$

$$\lambda_i = \left(\frac{1}{\lambda_t + a_8\beta} - \frac{a_9}{\beta^3 + 1} \right)^{-1} \quad (2)$$

where a_1 to a_9 are the constructive characteristic of the turbine, their value are $a_1 = 0.22$, $a_2 = 210$, $a_3 = 0.8$, $a_4 = 0$, $a_5 = 1$, $a_6 = 8$, $a_7 = 18$, $a_9 = 0.01$, β is the turbine blade's angle, λ_t is the tip-speed ratio.

The mechanical coupling is modeled using the two-mass model, which can be written as the following equations

$$\dot{\omega}_t = \frac{1}{2H_t}(T_t - K_s\theta - D_t\omega_t) \quad (3)$$

$$\dot{\omega}_r = \frac{1}{2H_g}(K_s\theta - T_e - D_g\omega_r) \quad (4)$$

$$\dot{\theta} = \omega_b(\omega_t - \omega_r) \quad (5)$$

where ω_t is the turbine rotational speed, ω_r is the rotor rotational speed, T_t is the turbine torque, T_e is the generator electrical torque, K_s is the torsional rigidity constant ($\frac{p.u}{rad}$), D_t is the turbine damping coefficient, D_g is the rotor damping coefficient, θ is the torsional angle, H_t is the inertial constant of the turbine and H_g is the inertial constant of the rotor (Ackermann, 2005).

The dynamic model of the induction generator used in this paper is modeled considering the dq0-axis and synchronous speed reference frame, all the parameters are expressed by per-unit system and the model is described by the following equations (Ackermann, 2005; Aguilar, 2016)

$$\frac{\dot{\lambda}_{ds}}{\omega_b} = -\frac{R_s}{\sigma L_s}\lambda_{ds} + \omega_s\lambda_{qs} + \frac{R_s k^2}{\sigma M}\lambda_{dr} - V_{ds} \quad (6)$$

$$\frac{\dot{\lambda}_{qs}}{\omega_b} = -\frac{R_s}{\sigma L_s}\lambda_{qs} - \omega_s\lambda_{ds} + \frac{R_s k^2}{\sigma M}\lambda_{qr} - V_{qs} \quad (7)$$

$$\frac{\dot{\lambda}_{dr}}{\omega_b} = -\frac{R_r}{\sigma L_r}\lambda_{dr} + (\omega_s - \omega_r)\lambda_{qr} + \frac{R_r k^2}{\sigma M}\lambda_{ds} - V_{dr} \quad (8)$$

$$\frac{\dot{\lambda}_{qr}}{\omega_b} = -\frac{R_r}{\sigma L_r}\lambda_{qr} - (\omega_s - \omega_r)\lambda_{dr} + \frac{R_r k^2}{\sigma M}\lambda_{qs} - V_{qr} \quad (9)$$

$$\sigma = 1 - k^2 \quad (10)$$

$$k^2 = \frac{M^2}{L_s L_r} \quad (11)$$

where the sub-index d, q, r and s stand for direct axis, quadrature axis, rotor e stator respectively, λ is the magnetic flux, k^2 is the coupling factor, σ is the dispersion factor, R_s is the stator resistance, R_r is the rotor resistance, ω_s is the dq0 axis speed which could be defined as rotational synchronous velocity, ω_r is the rotor rotational speed.

The converter used here is a back-to-back converter, which could be separated in the Rotor Side Converter (RSC), Grid Side Converter (GSC) and the DC-link. The equation that defines the DC-link dynamic is

$$\dot{V}_{dc} = \frac{\omega_b}{CV_{dc}}(P_r - P_g) \quad (12)$$

where V_{dc} is the DC-link voltage, C is the value of the capacitor, P_r is the active power flowing from the rotor side converter and P_g is the active power flowing to the grid. In steady-state neglecting the power losses, both powers will be balanced, and the value of $\dot{V}_{dc}$ will be zero. The system frequency is smaller than the converter switching frequency, thus, it is possible to represent the RSC using the fundamental frequency model, then the RSC can be express by:

$$\begin{cases} V_{dr} = m_{dr}V_{dc} \\ V_{qr} = m_{qr}V_{dc} \end{cases} , \forall\ 0 \leq m_{dr}^2 + m_{qr}^2 \leq m_{max} \quad (13)$$

where m_d and m_q are the modulation indexes represented in d-axis and q-axis. The GSC can be modeled as a current source, neglecting the converter current control droop dynamics, which is very fast.(Anaya-Lara et al., 2009; Rhode, 2019) Figure 1 represents the RSC control loop, which controls the active and stator reactive power. As shown in Figure 1, there is a maximum power point track (MPPT) that will be responsible for maintaining the maximum active power generation, the reference provided by MPPT is compared to the actual active power generation and the error is processed by a proportional-integrator controller which provides the i_q^* reference (Salles, 2009). The reactive power is compared to the reference, which generally is zero, and the error is compared in a proportional-integral controller that results in a i_d^* reference current. Both i_d^* and i_q^* are compared to the actual i_d and i_q, the error is processed by a PI controller, which enter in the current decoupling block. The transient value of I_g is obtained

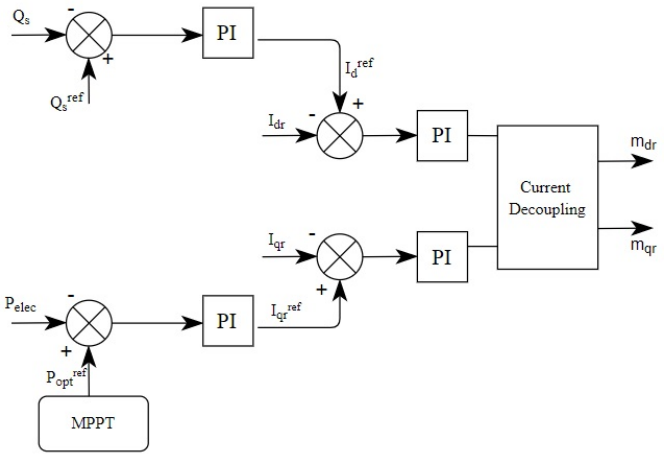

Figure 1. RSC control loop

through the GSC control loop. Figure 2 describes the grid side converter control loop, whose function is to maintain the DC-link voltage constant. The DC-link voltage control

loop employs a PI controller, which provides the direct-axis current reference. In general, the wind turbine works at unity power factor, so the reference of i_q^* in the GSC is zero. Both i_d^* and i_q^* are compared to the actual currents and the error is processed by a PI controller, and providing the d-q-axis voltage references (Salles, 2009).

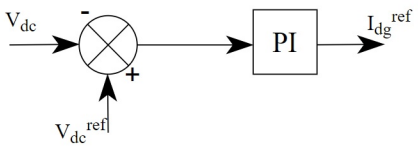

Figure 2. DC-link voltage control

3. REACTIVE POWER CONTROL STRATEGY

The National System Operator (ONS) in Brazil requires (ONS, 2019) that wind turbines do not disconnect from the system while the grid voltage sags remain inside the dashed area of Figure 3, which shows the LVRT condition for WT. Moreover, the WT should be capable of injecting reactive current while the grid voltage drop to $0.85p.u$, and the WT needs to have the ability to absorb reactive current while the grid voltage is over $1.1p.u$ as shown in Figure 4.

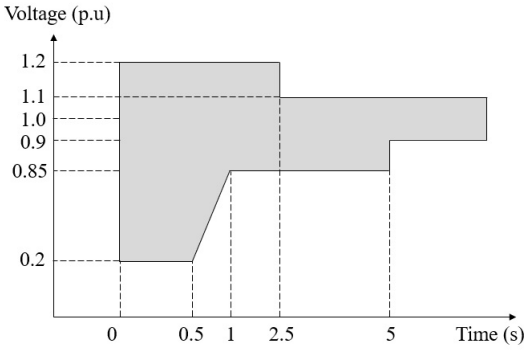

Figure 3. LVRT requirement for WT
Adapted from ONS (2019)

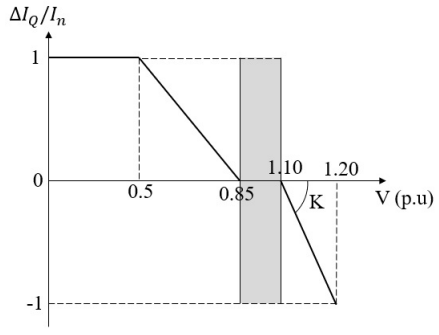

Figure 4. Reactive current injection requirement curve
Adapted from ONS (2019)

The Figure 4 shows a dashed area where the reactive current strategy should not act. When the voltage steps out of the dashed area, having its value above $1.1p.u$, the WT should absorb the reactive current from the grid. The opposite happens when the voltage drops below $0.85p.u$, the WT should have the capacity to provided reactive current to the grid. The ordinate axis is represented by

$$\Delta I_Q = I_Q - I_{Q0} \tag{14}$$

where ΔI_Q is the difference between I_Q and I_{Q0}, which are reactive current and reactive current before disturbance respectively, I_n is the rated current and K is the angle provided by the ONS. The reactive current injection and absorption are described by the following equations respectively

$$I_Q = 2.857(0.85 - V_s),\ 0.5p.u \leq V_s \leq 0.85p.u \tag{15}$$

$$I_Q = 10(1.1 - V_s),\ 1.1p.u \leq V_s \leq 1.2p.u \tag{16}$$

According to the equation (15), the amount of reactive current corresponding to the rated current should be provided when the voltage reaches $0.5p.u$. In case of a voltage event reaching $1.2p.u$ the WT should be able to absorb $1.0p.u$ of reactive current from the grid as described by the equation (16). For simplicity, in this paper we only consider the low voltage part of the reactive current injection curve. Following the strategy in (Asif et al., 2018). The GSC was not considered for reactive power injection as in (Asif et al., 2018) since our conditions do not include very low voltage levels that would trigger it. The reactive power reference is obtained as

$$Q_s^{ref} = \begin{cases} \frac{1}{0.35}(0.85 - V_s), & 0.5p.u \leq V_s \leq 0.85p.u \\ 1, & V_s < 0.5p.u \end{cases} \tag{17}$$

where Q_s^{ref} is the reactive power reference, and V_s is the grid voltage (Asif et al., 2018). The equation shows the maximum reactive power injection happens when the grid voltage drops below $V_s = 0.5p.u$ reaching the value of $Q_s^{ref} = 1p.u$, as described by the ONS see Figure 4.

4. SIMULATION

Simulations are performed using Matlab/Simulink for a DFIG-based WT of $20MW$ and $690V$ connected to the network in a machine infinite bus configuration as shown in Figure 5.

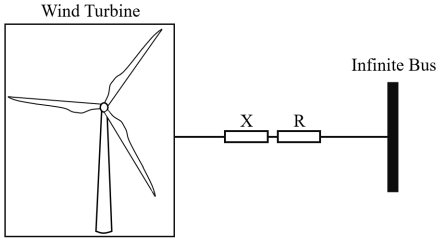

Figure 5. DFIG-based WT - single machine infinite bus configuration

In order to be able to analyze the efficiency of the grid voltage support by injecting reactive power from the wind turbine, the wind turbine is subjected to a symmetrical fault applied at its terminals. Crowbar protection (Simon et al., 2018) is not analyzed, so the fault is chosen to avoid its activation. The fault is applied in $t = 2.2s$, and is cleared in $t = 3.5s$. The event is simulated for three values of the wind power integration level (ρ), $\rho = 0.33$,

$\rho = 0.25$, and $\rho = 0.16$, and the X/R ratio will also be set to different values, $X/R = 1,\ 3$, and 5. The wind speed is considered constant during the simulation, the active power output in the operating condition is set to 0.8 $p.u$, and later varied to test the response to different active power output condition. The wind turbine operates with unity power factor during all simulations.

Figures 6 to 9 show the transient behavior of the wind turbine during the fault, comparing the cases with and without reactive current injection. In these simulations, $\rho = 0.25$ and $X/R = 5$. As shown in Figure 6, in the case without current injection, the voltage drops from $1.02p.u$ to $0.65p.u$ during a fault, recovering to the pre-fault value after fault removal. For the case with current injection, however, the voltage drops only to $0.73p.u$, for the same fault condition. This gain in the voltage level happened due to the reactive current injection strategy during the fault period. The impact on the voltage recovery after fault removal appears mainly as an over-voltage peak, which is due to the reactive power control loop dynamics. This dynamics can be seen in Figure 7. As the voltage drops, the current injection strategy modifies the reactive power control loop reference causing the DFIG to deliver reactive power to the grid, which, by its turn, improves the voltage level. At fault removal, even though the reactive power reference is instantly returned to zero, the time required for the actual reactive power to settle causes a peak in the voltage to appear.

During the fault, the total amount of current increases in the case of current injection, as shown in Figure 8, this is a consequence of the reactive power that the DFIG delivers to the grid in this case. On the other hand, after fault removal, the behavior of the total current is the opposite, being smaller in the case of current injection. This behavior of the total current can be understood from Figure 9 which shows the DFIG active power. The amount of active power has also increased during the fault, which happened due to the voltage value during the fault period also increased. Such increase in the active power, however, allows a larger portion of the available wind power to be transferred to the grid, so after the fault removal, there remains a smaller deviation to be corrected and the active power results smaller in the case of the current injection.

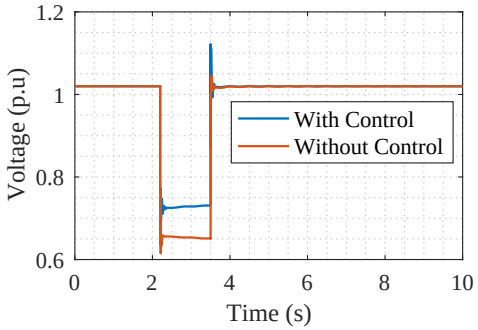

Figure 6. Voltage comparison - case with and without control

The performance of the reactive current injection strategy was also simulated for different values of the wind power integration level ρ ($\rho = P_n/S_{sc}$, the rated wind power per short circuit capacity ratio). The X/R ratio was maintained at the value of 5. Results are shown in the Figures 10 to 12. Figure 10 shows the influence of the wind power integration level on the performance of the reactive current injection strategy. The higher the integration level, the stronger the voltage sag during the fault. This shows that the efficiency of the grid support depends not only on the reactive power control but also on the connection characteristic that the WT is inserted. Notice from the Figures 10 and 11, they show the voltage and the reactive power relation to ρ, the higher the value of ρ, the higher the voltage drop and that is why the reactive power injected during the fault period is higher.

Since the reactive power injection has increase, the amount of current injected during the fault period by the wind turbine depends on the ρ value, a higher value of ρ result in a higher total current due to the influence of the grid

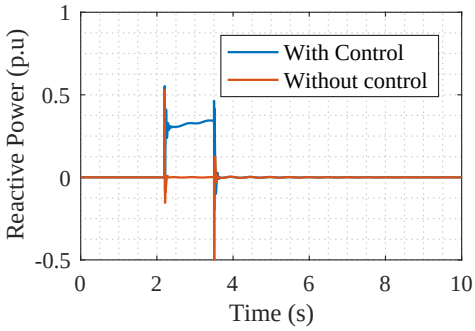

Figure 7. Reactive power comparison - case with and without control

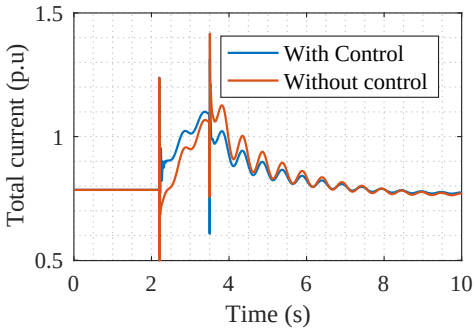

Figure 8. Total current comparison - case with and without control

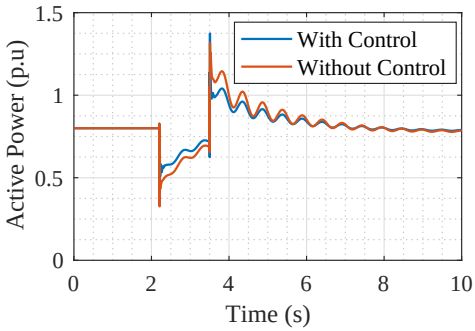

Figure 9. Active power comparison - case with and without control

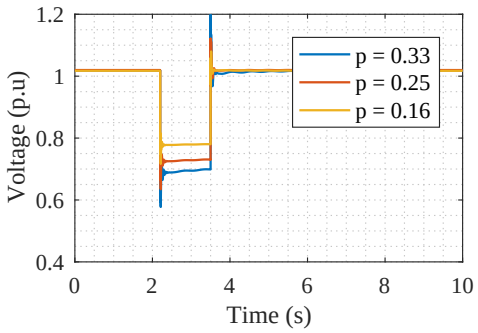

Figure 10. Voltage comparison - case varying ρ values

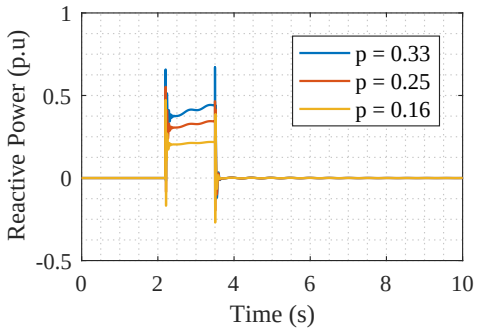

Figure 11. Reactive power comparison - case varying ρ values

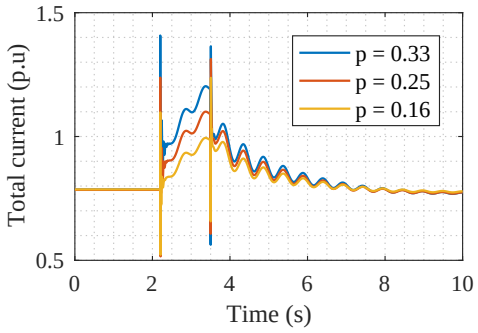

Figure 12. Total current comparison - case varying ρ values

system. Figure 12 shows that higher values of ρ, the higher current value will be injected by the WT. When the value of ρ is lower, result in a higher value of active power during the fault period. But there is not much difference in the active power for the three values of ρ. While the reactive power has the inverse effect, the higher value of integration level, the higher the reactive power injected during the fault as shown in Figure 11.

The current injection strategy was also simulated for different values of the X/R ratio. For these simulations, the wind power integration level was maintained at 0.25. Figures 13 to 15 show, respectively, the voltage, reactive power and, total current behavior for $X/R = 1, 3$, and 5. Since the wind turbine operates with unity power factor, the voltage at the operating point changes as the X/R ratio changes. When the system approaches to distribuition system characteristics and the lower the X/R ratio gets, the voltage reaches higher values, including during the fault period, as shown in Figure 13.

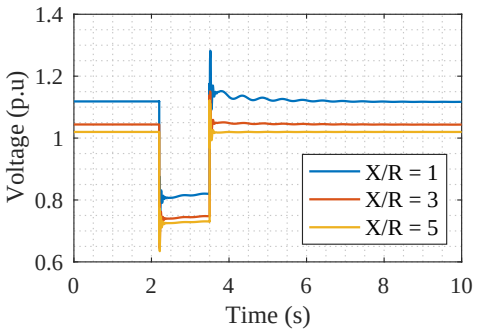

Figure 13. Voltage comparison - case varying X/R values

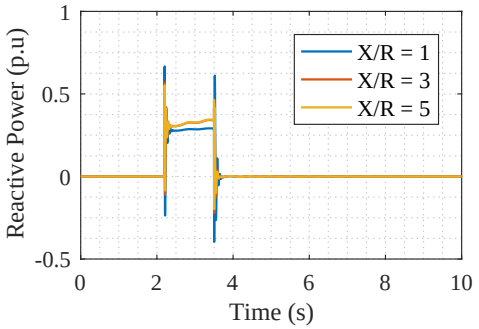

Figure 14. Reactive power comparison - case varying X/R values

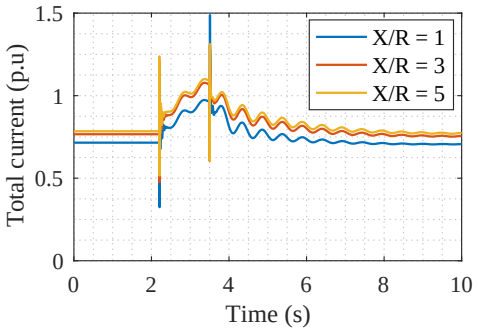

Figure 15. Total current comparison - case varying X/R values

The reactive and active power have not shown a considerable difference as voltage by varying those three values of X/R ratio. Figure 14 shows the reactive power response for the three values of X/R and they are very similar to each other when X/R assumes either 3 or 5, but with a considerable difference in the $X/R = 1$. The behavior of active power when the value of X/R is varied does not show considerable difference to the reactive current injection strategy, and, the three cases are very close. Hence, the behavior of active power maintain the same by varying the X/R ratio, not showing any advantage during the fault in transmission system.

Finally, the reactive current injection strategy was simulated for different values of wind turbine active power output. The X/R ratio was set to five and the ρ value set to one quarter. Figure 16 to 18 show, respectively, the voltage, reactive power and, total current behavior when

the simulated system is submitted to the reactive current injection strategy.

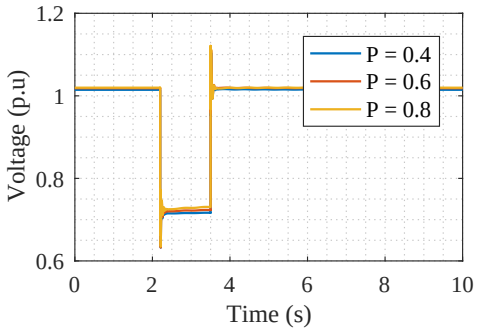

Figure 16. Voltage comparison - case varying active power operation values

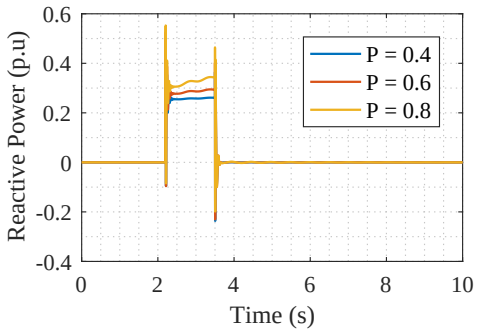

Figure 17. Reactive power comparison - case varying active power operation values

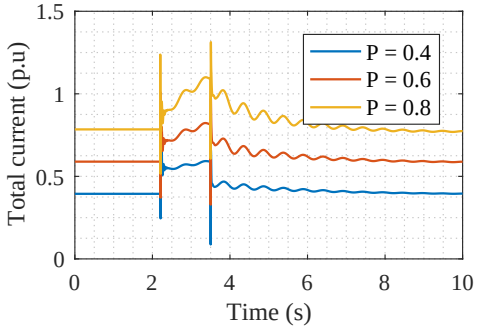

Figure 18. Total current comparison - case varying active power operation values

As Figure 16 shows, the voltage behavior for different values of active power output, for the three cases the voltage drop was considerable similar, that is, the drop value is almost the same. The value of reactive power during the fault period for the three cases are slightly distinct, the higher the operating point active power, the higher the reactive power attained during the fault period as shown in figure 17. As for the total current, the behavior are very close in the three cases of active power value, the different relies on the initial value as show in figure 18.

5. CONCLUSION

The reactive current injection strategy improved the voltage level during the fault, contributing to system voltage support. Moreover, there is a benefit in the DFIG active power transfer to the grid, whose value had increased during the fault, and had decreased in the post-fault period, thus reducing deviations from the operating point. The amount of total current increased during the fault because of the reactive current injection strategy.

The reactive current injection strategy is almost not affected by changing the wind farm operating point, but its effectiveness is affected by varying either the value of integration level (ρ) or the X/R ratio of the grid impedance. For larger values of wind power integration levels, the same fault requires more reactive current injection, since the terminal voltage dips to lower values. The value of the X/R ratio impacts the voltage operating condition of the wind farm when operating with unity power factor. This also affects the voltage level during the fault and so, the amount of reactive current injection. However, such injection is almost the same for X/R values higher than 3. Hence, for connections to the transmission system, the reactive current injection strategy will have the same effectiveness.

REFERENCES

Ackermann, T. (2005). *Wind Power In Power Systems*. John Wiley & Sons. doi:10.1002/9781119941842.ch44.

Aguilar, M.E.B. (2016). Sintonia dos Controladores para Aerogeradores de velocidade variável com geradores de indução de dupla alimentação utilizando um algoritmo meta-heurístico de inteligência coletiva.

Anaya-Lara, O., Jenkins, N., Ekanayake, J., Cartwright, P., and Hughes, M. (2009). *Wind Energy Generation Modelling and Control*. John Wiley & Sons.

Asif, M., Bux, R., and Memon, R.A. (2018). Improved RSC-GSC decoupled and LVRT control strategies of DFIG-based wind turbine. In *2018 International Conference on Electrical Engineering, ICEE 2018*. Institute of Electrical and Electronics Engineers Inc. doi:10.1109/ICEE.2018.8566875.

Kim, J., Muljadi, E., Park, J.W., and Kang, Y.C. (2016). Adaptive Hierarchical Voltage Control of a DFIG-Based Wind Power Plant for a Grid Fault. *IEEE Transactions on Smart Grid*, 7(6), 2980–2990. doi:10.1109/TSG.2016.2562111.

Nycander, E. and Söder, L. (2018). Review of European Grid Codes for Wind Farms and Their Implications for Wind Power Curtailments. *17th International Wind Integration Workshop*, (October), 1–7. URL `http://www.diva-portal.org/smash/record.jsf?pid=diva2:1257541`.

ONS (2019). Requisitos técnicos mínimos para a conexão às instalações de transmissão. Submódulo 3.6.

Rhode, T. (2019). Interação dinâmica de aerogeradores de indução dfig e fsig conectados em um mesmo alimentador de distribuição.

Salles, M.B.d.C. (2009). Modelagem e análise de geradores eólicos de velociade variável conectados em sistemas de energia elétrica.

Simon, L., Naina, P.M., and Swarup, S. (2018). Transient Modeling and Control of DFIG with Fault Ride Through Capability. *International Conference on Innovative Smart Grid Technologies, ISGT Asia 2018*, 928–933. doi:10.1109/ISGT-Asia.2018.8467879.